[4]S. U. Chung, O. I. Dahl, L. M. Hardy, R. I. Hess, G. R. Kalbfleisch, J. Kirz, D. H. Miller, and G. A. Smith, Phys. Rev. Letters 12, 621 (1964); D. J. Crennell, U. Karshon, K. W. Lai, J. M. Scarr, and I. O. Skillicorn, *ibid.* 20, 1318 (1968).

[5]K. J. Foley, W. A. Love, S. Ozaki, E. D. Platner, A. C. Saulys, E. H. Willen, and S. J. Lindenbaum, Phys. Rev. Letters 26, 413 (1971).

[6]K. J. Foley, W. A. Love, S. Ozaki, E. D. Platner, A. C. Saulys, E. H. Willen, and S. J. Lindenbaum (unpublished).

[7]K. Gottfried and J. D. Jackson, Nuovo Cimento 33, 309 (1964).

[8]J. D. Jackson, Nuovo Cimento 34, 1644 (1964).

[9]This shape is very close to the functional form suggested by Quigg and von Hippel (Ref. 3, p. 477):

$$\Gamma(m) = \Gamma_0 \frac{\rho(q)}{\rho(q_0)} ,$$

where

$$\rho(q) = \frac{qR}{|H_2^{(1)}(qR)|^2} .$$

$H_2^{(1)}$ is the Hankel function of the first kind.

[10]A more refined Monte Carlo calculation of the acceptance has modified these numbers slightly from those published earlier (Ref. 5).

[11]In order to estimate the possible size of background, we have fitted the data over the mass region 1.1–1.5 GeV allowing a linear background term. After correction for the acceptance, a background level of 1.6 ± 0.7 events/bin was found, while the peak height is ≈30 events/bin.

[12]J. L. Rosner, in *Phenomenology in Particle Physics*, edited by C. B. Chiu, G. C. Fox, and A. J. G. Hey, (Caltech, Pasadena, 1971).

[13]F. James and M. Roos, CERN Computer Program Library Reports No. D506 and No. D516 (unpublished).

[14]R. H. Dalitz, Nucl. Phys. 87, 89 (1966); S. U. Chung (unpublished).

[15]G. Grayer, B. Hyams, C. Jones, P. Schlein, W. Blum, H. Dietl, W. Koch, H. Lippmann, E. Lorenz, G. Lütjens, W. Männer, J. Meissburger, U. Stierlin, and P. Weilhammer, Phys. Letters 34, B333 (1971); D. Bowen, D. Earles, W. Faissler, D. Garelick, M. Gettner, M. Glaubman, B. Gottschalk, G. Lutz, J. Moromisato, E. I. Shibata, Y. W. Tang, E. von Goeler, H. R. Blieden, G. Finocchiaro, J. Kirz, and R. Thun, Phys. Rev. Letters 26, 1663 (1971); D. Underwood, G. Conforto, M. A. Kramer, R. Prepost, D. H. Tompkins, M. S. Witherell, A. W. Key, and R. M. Mobley, Bull. Am. Phys. Soc. 17, 64 (1972) and private communication with M. A. Kramer; D. M. Binnie, L. Camilleri, A. Duane, A. R. Faruqi, D. A. Garbutt, W. G. Jones, M. E. Kay, M. Lewis, P. J. Nicholson, I. Siotis, P. N. Upadhyay, J. G. Wilson, I. F. Burton, S. G. Frank, R. George, M. Haque, and J. G. McEwen, Phys. Letters 36B, 257 (1971).

[16]M. Basile, P. Dalpiaz, P. L. Frabetti, T. Massam, F. Navach, F. L. Navarria, M. A. Schneegans, and A. Zichichi, Lett. Nuovo Cimento 4, 838 (1970); K. W. J. Barnham, G. S. Abrams, W. R. Butler, D. G. Coyne, G. Goldhaber, B. H. Hall, J. MacNaughton, and G. H. Trilling, Phys. Rev. Letters 26, 1494 (1971); D. J. Crennell, H. A. Gordon, K. W. Lai, and J. M. Scarr, Phys. Letters 35B, 185 (1971); D. M. Binnie, L. Camilleri, A. Duane, D. A. Garbutt, J. R. Holmes, W. H. Jones, J. Keyne, M. Lewis, I. Siotis, P. N. Upadhyay, I. F. Burton, R. George, and J. G. McEwen, *ibid.* 36B, 537 (1971); I. J. Bloodworth, W. C. Jackson, J. D. Prentice, and T. S. Yoon, Nucl. Phys. B37, 203 (1972).

PHYSICAL REVIEW D VOLUME 6, NUMBER 3 1 AUGUST 1972

Measurement of the Differential Cross Section for $\pi^- p \to n\pi^0$ at 317, 452, and 491 MeV/c*

P. A. Berardo,† R. P. Haddock, B. M. K. Nefkens, L. J. Verhey,‡ and M. E. Zeller§
University of California, Los Angeles, California 90024

and

A. S. L. Parsons‖ and P. Truoel**
Lawrence Berkeley Laboratory, University of California, Berkeley, California 94720
(Received 27 March 1972)

Seventeen differential cross sections of the pion-nucleon charge-exchange reaction have been measured at total center-of-mass energies of 1245, 1337, and 1363 MeV. Most measurements are based on the neutron-photon coincidence method, using carefully calibrated neutron counters and an efficient, large-area photon detector. The results are used to test the predictions of charge independence, with which they agree. The results also confirm the Ayed-Bareyre-Sonderegger phase-degeneracy hypothesis at $\tilde{\theta}_{\pi^0} = 180°$.

I. INTRODUCTION

We have measured the differential cross sections for the pion-nucleon charge-exchange (CEX) reaction,

$$\pi^- p \to \pi^0 n ,$$

at 317-, 452-, and 491-MeV/c pion momenta in the laboratory, corresponding to $\tilde{E} = 1245$-, 1337-, and 1363-MeV center-of-mass total energies.

These data were obtained in the course of another experiment in which the differential cross sections for radiative pion capture in flight[1] (REX reaction),

$$\pi^- p \to \gamma n,$$

were measured. We believe these data are of interest for four reasons. First, the difficulties of determining the small REX cross section forced us to employ a technique which has removed or reduced some of the systematic errors associated with previous CEX measurements.[2-8] Second, our data at $\tilde{E} = 1245$ MeV are close to the peak of the $\Delta(1236)$, where there is a paucity of data. Third, there is a need for more CEX data in the phase-shift analysis of the π-N system, as has been emphasized many times.[9] Extensive phase-shift analyses of the π-N system below 2 GeV have been undertaken by several groups.[10-12] Shown in Fig. 1 is a comparison between four phase-shift predictions for the CEX differential cross sections at $\tilde{E} = 1362$ MeV; differences of more than a factor of 1.5 can be observed. This illustrates clearly the need for CEX data in our energy range. Fourth, the CEX data can be used to test the hypothesis of isospin conservation via the triangle inequalities.[13]

A brief historical review of the experimental methods follows in this section. Section II deals with theoretical considerations. Sections III, IV, and V describe our experimental arrangement, analysis, and results, respectively, and conclusions are discussed in Sec. VI.

The earliest charge-exchange differential cross sections[2-6] in our energy region were derived from measurements of the angular distribution of

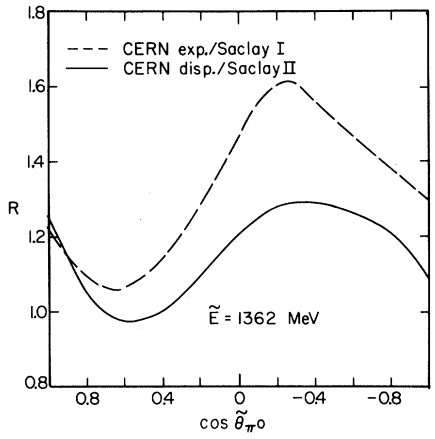

FIG. 1. Ratio R of predictions for $\pi^- p \to \pi^0 n$ based on recent phase-shift analyses. CERN disp. and exp. refer to the dispersion-relations-type and experimental-type phase shifts of Ref. 10. Saclay I and II refer to the minimum path and minimum surface solutions of Ref. 11.

single photons. The principal difficulty of this method is the unfolding of the energy dependence of the photon detection efficiency. Also, at high energies, there are uncertainties in background subtraction due to the production of additional π^0's.

A more direct method, used more recently,[7,8] has been to detect the final-state neutron and to identify a charge-exchange neutron by its unique energy. This technique is prone to systematic errors arising from the uncertainties in neutron detection efficiency. The most recent measurements in this energy region[8] utilized neutron counters which were calibrated at only one neutron energy with 10% precision, while theoretical calculations were used to predict the efficiency over the full range of neutron energies. An earlier measurement[7] relied completely on the calculation of the neutron detection efficiency. The accuracy of the second method of measuring CEX cross sections is further limited by the random background in the neutron detector, particularly at forward π^0 angles, where the neutron energy is low and the counter biases must be set correspondingly low. When $\tilde{E} > 1300$ MeV and $\tilde{\theta}_{\pi^0} > 120°$, the REX reaction is a non-negligible correction to the CEX cross sections. We have measured the REX contribution directly.

Our method is a combination of the above techniques, namely, a coincidence measurement of the neutron and one photon from π^0 decay. The CEX events are identified by the time of flight of the neutron, and the random background is reduced to a negligible level by requiring the detection of a photon. This background reduction is particularly important for large π^0 angles at the higher energies, where the CEX cross sections are small. The energy-dependent efficiency of our neutron counter array has been accurately measured over the entire range of detected neutron energies.[14] Our photon detector contained ten radiation lengths. The efficiency for shower detection is about 98% and nearly energy-independent over the range of interest, $150 < E_\gamma < 300$ MeV. Our main source of uncertainty is the solid-angle acceptance for a photon from π^0 decay. Besides the n-γ coincidence technique used for all 17 points, we determined 10 of these points in a separate experiment, using only the neutron time of flight. These independent measurements provide an excellent check on our determination of the solid angle and the efficiency of the photon detector.

II. THEORY

Under the assumption of isospin conservation, the amplitudes for the three experimentally accessible processes in π-N scattering may be expressed in terms of two isospin amplitudes:

$$A(\pi^+p \to \pi^+p) \equiv A^+ = A_{3/2}, \tag{1a}$$

$$A(\pi^-p \to \pi^-p) \equiv A^- = \tfrac{2}{3}A_{1/2} + \tfrac{1}{3}A_{3/2}, \tag{1b}$$

$$A(\pi^-p \to \pi^0n) \equiv A^0 = -\tfrac{1}{3}\sqrt{2}\,(A_{1/2} - A_{3/2}). \tag{1c}$$

Three experiments are necessary to determine the magnitude and relative phase of the two isospin amplitudes. It follows directly from Eq. (1) that the following relation must hold:

$$\sqrt{2}\,A^0 = A^+ - A^-. \tag{2}$$

This equality implies two constraints on the cross section, namely,

$$(\sqrt{\sigma^+} - \sqrt{\sigma^-})^2 < 2\sigma_0 < (\sqrt{\sigma^+} + \sqrt{\sigma^-})^2, \tag{3}$$

called the triangle inequalities. The constraints hold for all angles. A measurement of all three π-N scattering processes at the same energy and angle can thus be used to test isospin conservation in π-N scattering. A special angle to consider is 180°, since the contribution of the spin-flip amplitude vanishes there. Törnqvist[15] has noted that some of the data in the energy region $1300 < \tilde{E} < 1600$ MeV, when extrapolated to 180°, and when taken at face value, show a slight violation of the triangle inequalities. Ayed, Bareyre, and Sonderegger[16] (called ABS here) have interpreted the published data differently. They assert that at 180° the available data are consistent with the lower limit of the triangle inequalities in the region $1230 < \tilde{E} < 2100$ MeV and probably at all energies. The spectacularly low CEX cross section near $\tilde{E} = 1390$ MeV and $\tilde{E} = 1600$ MeV, where the π^+ and π^- cross sections are equal, is certainly impressive evidence in favor of the ABS hypothesis. When the experimental data are consistent with the lower bound of the triangle inequalities there are three possibilities: $A_{3/2} >> A_{1/2}$, or $A_{1/2} >> A_{3/2}$, or the relative phase between $A_{3/2}$ and $A_{1/2}$ is 0°. ABS obviously chose the last possibility. Our data, lying in the region where Törnqvist saw a possible isospin violation, are well suited for testing the triangle inequalities over the full angular region; also, they can determine whether the ABS phase degeneracy holds only at 180°.

An uncertainty in all tests of isospin conservation is caused by the Coulomb interaction, which does not conserve isospin. The Coulomb effects have not been calculated rigorously, but estimated, using potential models with an uncertain range of validity. Oades[17] estimates that the total effect of Coulomb corrections in the backward cross sections at $\tilde{E} \simeq 1230$ MeV is 1% or 2%. At the present level of experimental accuracy, Coulomb effects are unimportant in our energy range.

III. EXPERIMENTAL ARRANGEMENT

A. Beam

The experiment was performed at the 184-in. synchrocyclotron of the Lawrence Berkeley Laboratory. The beam transport system made a triply focused image of a beryllium target in the internal beam of the synchrocyclotron upon a liquid-hydrogen (LH) target 14 m away. Beam tuning was achieved by varying the internal target position and beam transport magnet currents.

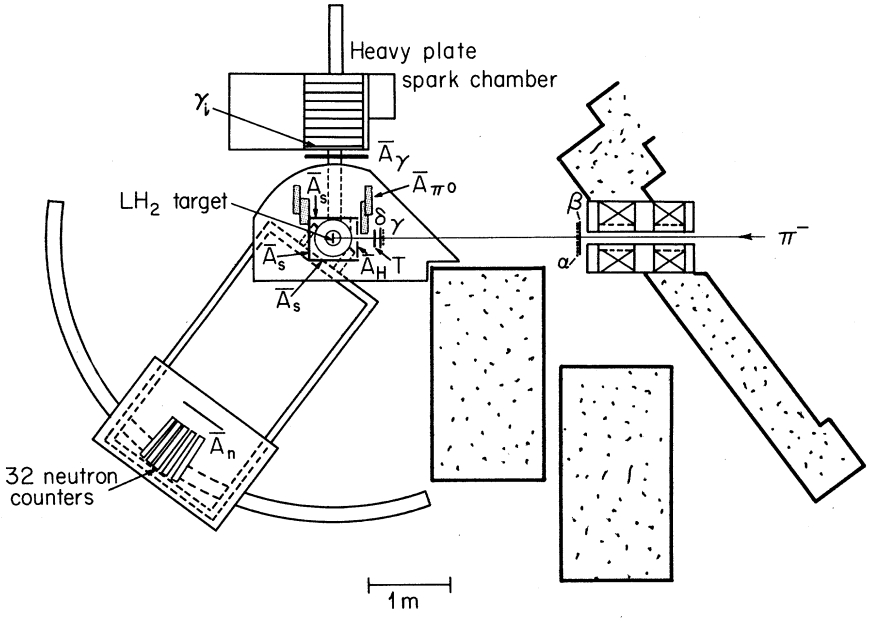

FIG. 2. Arrangement of detection apparatus.

TABLE I. Parameters of our pion beams. The beam contamination consists of electrons, on-momentum muons, $P_\mu = P_\pi$, and off-momentum muons, $P_\mu \neq P_\pi$.

c.m. energy $\tilde{E}$ (MeV)	Lab mom. P_π (MeV/c)	Momentum spread $\Delta P/P$	Rate π^-/sec	Contamination e^-	$\mu^-(P_\mu = P_\pi)$	$\mu^-(P_\mu \neq P_\pi)$	Total
1245	317 ± 6	±3.5%	5.5×10^5	2%	4%	5%	(11 ± 3)%
1337	452 ± 5	±3.3%	4.5×10^5	1%	2%	3.4%	(6.4 ± 1.7)%
1363	491 ± 5	±3.3%	2.5×10^5	1%	2%	2.7%	(5.7 ± 1)%

The trajectories of the pions entering the LH target were defined with a hodoscope system of 37 plastic scintillator counters, arranged in four planes, α, β, γ, and δ. (See Fig. 2.) The hodoscope determined the incident pion angle to $\pm\frac{1}{4}^\circ$ and the pion position to ±6 mm at the LH target. Further definition of the incident beam was made with another beam counter, T, used for timing purposes also. The final element in the beam counter telescope was an anticounter with a hole, $\bar{A}_H$. The beam momentum, spread, rate, and contamination are given in Table I. They are discussed in more detail in the forthcoming paper on the REX reaction.[18]

B. Target

The liquid-hydrogen target flask was a vertical cylinder, 10 cm high × 10 cm in diameter. The flask was divided symmetrically by a vertical Mylar membrane which was normal to the beam. This allowed the two halves to be filled independently so that runs could be made with either a full or half-full target. At most points, we chose to run with half-full target, to keep the uncertainty of the interaction point to a minimum.

C. Detection Apparatus

The experimental apparatus is shown in Fig. 2. The LH target was surrounded on four sides by anticoincidence counters: in the front by $\bar{A}_H$, downstream by $\bar{A}_s$, and left and right by two other $\bar{A}_s$. The anticounters suppressed triggering the system on charged particles that came out of the LH target, thus eliminating random coincidences due to elastic pion scattering in the LH target and straight-through beam particles. The last feature excluded cases where two pions came within the resolving time of our beam coincidence circuit. An incoming pion was defined by a coincidence between the four hodoscope planes, the timing counter T in front of the target, and no count in $\bar{A}_H$.

The heart of the experiment was the neutron detector. Details of the construction and calibration of the detector are given elsewhere.[14] The detector consisted of an array of 32 cylindrical liquid scintillator counters, each 46 cm long and 7 cm in diameter. The individual elements were arranged in a semiclose packed array, as shown in Fig. 3, with the axis of each cylinder lying along a radius to the target when the detector was at its normal 3.7-m radius from the target. To avoid triggering the neutron counters on the few charged particles from the target not eliminated by $\bar{A}_s$, a pair of plastic counters, labeled $\bar{A}_N$, covered the face of the neutron counters. The neutron array was mounted on a cart such that both the angle and the distance from the target could be easily changed.

The efficiency of the neutron counter array was measured in a separate experiment.[14] The method used was that of elastic neutron-proton scattering. The recoil proton energy and angle were measured in a range telescope, thereby determining the energy and angle of the scattered neutron. The quantity that was actually measured in the calibration experiment was the neutron counter efficiency, modified by scattering of the neutrons in the target and neutron counters. Separate measurements were made of the probability for cross scattering of neutrons or their recoil protons between counters in the array, or out of the array.

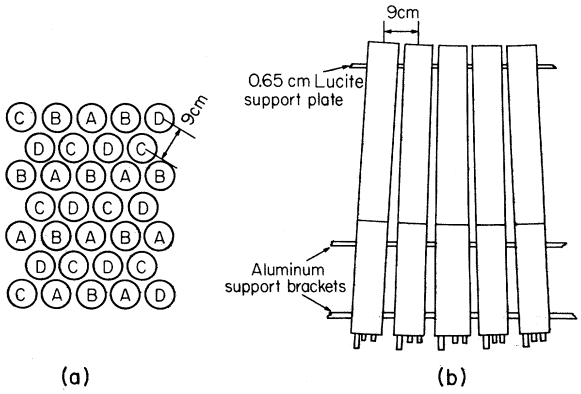

FIG. 3. Geometrical arrangement of neutron counters. Figure 3(a) is the front view as seen by the neutrons. Each neutron counter is assigned to one of four independent time-to-height converters, as indicated by a letter on each counter. Figure 3(b) is the top view.

Neutral cross scattering, defined as the scattering of a neutron from one counter to another (but detection in the second counter only) averaged 17% for our array. Charged cross scattering averaged 13%; this occurs when a neutron or a recoil proton triggers two adjacent counters. A Monte Carlo program which simulated the calibration conditions was used to obtain the efficiency per cm of possible path length of a nonscattered neutron from the above measurements. The hydrogen target used in the efficiency measurement was the same as that of the CEX and REX experiment. The absolute efficiency was between 0.5 and 0.4 in the energy range of our experiment, and it was determined to an accuracy of about ±3% of the absolute efficiency. Corrections for neutron scattering in the hydrogen target were included in the absolute efficiency.

The photons were detected in a heavy-plate optical spark chamber. The chamber consisted of 10 modules. The thickness of each one was one radiation length. Each module had five metal plates, forming a four-gap module. Four of the plates were laminated lead and stainless steel, while the fifth was all stainless steel. The active area of each module was 76×76 cm. Interspersed between the front nine modules were eight pairs of plastic scintillator trigger counters, γ_i. In front of the first module was a pair of counters, $\bar{A}_\gamma$, which were in anticoincidence.

The γ detector was viewed by a camera from the top and side, and the resulting photographs were scanned off-line with an automatic vidicon system.[19] The handling of the spark chamber data and the photon detection efficiency are discussed in detail in Ref. 18. The entire γ detector with its optics was mounted on wheels and could be moved in both radius and angle.

D. π^0 Anticounters

Eight lead-scintillator sandwich γ detectors, designated $\bar{A}_{\pi 0}$ in Fig. 2, were mounted around the target. These were inserted for the benefit of the REX experiment, as they were sometimes used in anticoincidence to discriminate against CEX events. For these runs, extra care was necessary in the analysis of the charge-exchange cross sections.

The efficiency of the π^0 anticounters was determined in a separate calibration experiment performed in a tagged photon beam at the Caltech Synchrotron.[20] Typical results which we obtained were (30± 7)% at 25 MeV, (67±4)% at 50 MeV, and (91± 2)% at 100 MeV. The uncertainty in this efficiency contributed to the error in the final cross section values for those points where the π^0 anticounters were in the trigger.

E. Triggering and Electronics

An event trigger was defined as

$$\alpha\beta\gamma\delta T\bar{A}_H\bar{A}_s n\gamma_i\gamma_j\bar{A}_n\bar{A}_\gamma(\bar{A}_{\pi 0}).$$

$\gamma_i\gamma_j$ means that two or more planes of scintillator in the gamma detector were required. This requirement ensured that the photon shower persisted for at least a radiation length. The time gate for neutron detection was such that the time of flight of the neutron had to be within about ±35 nsec of the time expected for the REX neutron. The CEX neutrons are always inside this time interval. Our 32 neutron counters were arranged in four independent groups, called A, B, C, and D, each with its own time-to-height converter. The as-

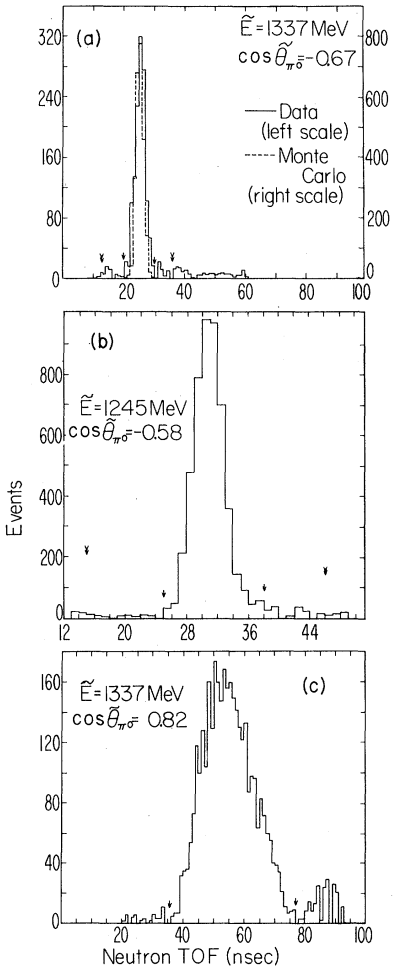

FIG. 4. Neutron time-of-flight (TOF) spectra, after subtraction of a small target-empty background. The triggering mode is an n-γ coincidence. The dashed curve in Fig. 4(a) is a Monte Carlo simulation. Single arrows indicate the CEX region. The region between single and double arrows is used for background evaluation.

signment of individual neutron counters to each group is indicated in Fig. 3(a). Details on the electronics are given in the papers describing the radiative capture experiment.[18]

The events were obtained in two types of runs. In the normal (REX) data runs the trigger which was discussed above was used and CEX events were taken simultaneously with REX events. We shall refer to this triggering mode as the "n-γ coincidence method." At ten points we also took events for which only a neutron was required by removing the $\gamma_i\gamma_j\overline{A}_\gamma\overline{A}_{\pi 0}$ requirement in the trigger. This triggering mode will be called "n-only." This type of run was important to check the Monte Carlo calculation of the solid angle for detection of one γ from the π^0 decay and the product of efficiency and solid angle of the $\overline{A}_{\pi 0}$ counters. In most of the REX-type runs the $\overline{A}_{\pi 0}$ counters were in anticoincidence in the main trigger. In a few runs the $\overline{A}_{\pi 0}$ counters were latched for recording on tape and this information could later be used or ignored.

In all our runs, the counter information and neutron time of flight of all events which passed our trigger criteria were recorded on magnetic tape by a PDP-5 computer for off-line analysis.

IV. DATA ANALYSIS

The number of charge-exchange events was determined from the measured neutron time-of-flight spectrum by subtracting, bin by bin, the small empty-target background. Figures 4(a)–4(c) show typical spectra of data minus empty-target background obtained when the trigger had a γ in coincidence with the neutron. The total background, including $\pi^- p \to n\pi^0\pi^0$, is normally very small (2–3%); in the worst case, at $\tilde{E} = 1363$ MeV and $\cos\tilde{\theta}_{\pi 0} = -0.87$, it is 7%. In the cases where the coincident γ condition is removed, the random background can be much larger, as shown in Figs. 5(a)–5(c).[21] The solid curves in Fig. 5 are fits to the spectra using Gaussian distributions on a linear background. The fits are used to evaluate the number of counts in the peak. σ_t is the full width at half height of the CEX peak expected from kinematics, counter length, electronic resolution, etc. The peak at earlier times is the photon "prompt" peak. In Fig. 4(a) is shown a typical neutron time-of-flight distribution along with the shape predicted by a Monte Carlo program. The experimental spectrum is slightly wider at the base than the one predicted by the Monte Carlo. This is due to the imperfection in the determination of the zero time in each of the 32 neutron counters and due to neutrons that scattered in the hydrogen. We estimate the uncertainty in the CEX cross section due to

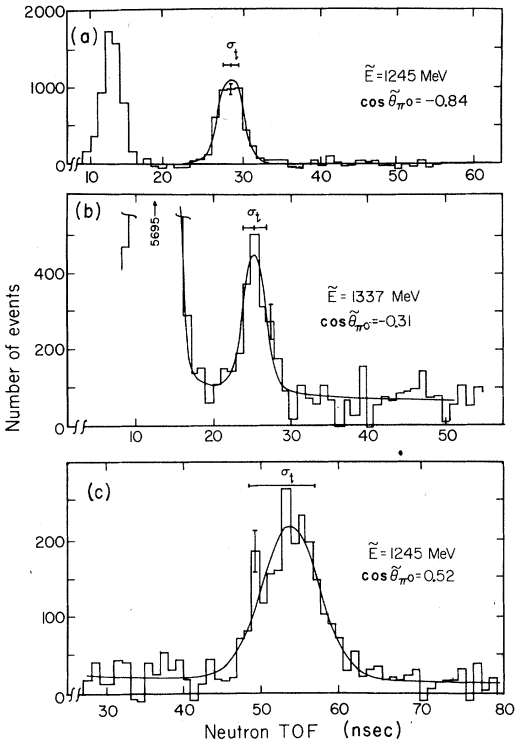

FIG. 5. Same as Fig. 4 except that the triggering mode is the "neutron-only CEX" mode. The solid line is discussed in the text.

neutron scattering in the hydrogen target to be less than 1%.

In addition to the number of events, the analysis must deal with the problems of solid angle and efficiency. The neutron solid angle is defined as the geometrical solid angle subtended at the target by all the neutron counters.

The Monte Carlo program used to analyze the CEX and REX experiments included the following for the neutron: (1) a means of calculating the efficiency of a single counter as a function of distance from the LH_2 target, (2) a model of the neutral and charged cross scattering between neutron counters in our array, and (3) corrections for neutron scattering in the LH_2 target structure and surrounding anticounters.

To evaluate the γ solid angle one must determine the probability for one γ from π^0 to enter the fiducial region of the spark chamber, where the efficiency for detection is known, and for the other γ not to trigger an $\overline{A}_{\pi 0}$ counter. This last condition was of course ignored in the cases where the $\overline{A}_{\pi 0}$'s were not in the trigger. A Monte Carlo program, which simulated the entire experiment, was used to calculate the γ solid angle. This number is typically between $\frac{1}{6}$ and $\frac{1}{3}$.

TABLE II. Our experimental CEX results and important parameters in the cross-section calculation. The parameters are defined in the text. The spread in $\cos\tilde{\theta}_{\pi^0}$ is due to the width of our neutron counter array. The error quoted in the cross section is the normalization and relative error combined in quadrature. In the cases where there are two measurements, the last column gives the weighted mean and corresponding uncertainty.

$\tilde{E}$ (MeV)	$\cos\tilde{\theta}_{\pi^0}$	Method	N_{evts}	N_{REX}	$\bar{t}\rho$ (10^{23} cm^{-2})	π^*_{in} (10^6)	$d\Omega_n$ (sr)	J	f^*	Relative error	$\frac{d\sigma}{d\tilde{\Omega}}$ (mb/sr)	$\frac{d\bar{\sigma}}{d\tilde{\Omega}}$ (mb/sr)
1245	0.52±0.08	$n\gamma$	4525±80	460±35	3.782	7084	9.166	1.925	0.0320±0.0022	5.2%	2.68 ±0.19	2.68 ±0.19
	0.15±0.10	$n\gamma$	2551±70	330±25	1.891	6948	9.166	2.595	0.0408±0.0026	5.0%	1.74 ±0.12	1.81 ±0.11
	0.15±0.10	n	1111±72	18±5	3.782	200.3	9.166	2.595	0.313 ±0.014	6.1%	1.93 ±0.15	
	−0.22±0.10	$n\gamma$	3518±70	390±45	1.891	8336	9.166	3.19	0.0367±0.0024	5.1%	1.85 ±0.13	1.85 ±0.13
	−0.58±0.09	$n\gamma$	4885±110	330±65	1.891	8674	9.166	3.69	0.0324±0.0023	5.8%	2.53 ±0.19	2.71 ±0.16
	−0.58±0.09	n	2524±117	16±4	3.782	225	9.166	3.69	0.304 ±0.015	4.6%	2.86 ±0.19	
	−0.84±0.06	$n\gamma$	5011±81	250±60	3.782	2323	9.166	4.035	0.0355±0.0025	5.5%	4.12 ±0.30	4.20 ±0.23
	−0.84±0.06	n	3919±240	40±10	3.782	214	9.166	4.035	0.301 ±0.015	6.3%	4.30 ±0.34	
1337	0.82±0.06	$n\gamma$	3345±68	460±54	3.716	8440	13.199	1.15	0.0162±0.0018	10.3%	3.74 ±0.42	3.24 ±0.31
	0.82±0.06	n	1824±205	52±9	3.716	499	13.199	1.15	0.227 ±0.021	13.8%	2.77 ±0.40	
	0.41±0.09	$n\gamma$	2857±70	250±42	1.858	12480	9.166	2.18	0.0456±0.0030	5.8%	1.23 ±0.09	1.27 ±0.07
	0.41±0.09	n	1310±99	16±4	3.716	400	9.166	2.18	0.329 ±0.011	7.1%	1.32 ±0.11	
	0.04±0.10	$n\gamma$	4981±102	354±35	1.858	19200	9.166	2.86	0.101 ±0.0064	5.2%	0.489±0.033	0.489±0.033
	−0.31±0.09	$n\gamma$	1566±50	380±30	1.858	20400	9.166	3.43	0.0377±0.0026	6.2%	0.263±0.020	0.262±0.019
	−0.31±0.09	n	1324±210	50±8	3.716	1400	9.166	3.43	0.304 ±0.011	15.8%	0.256±0.042	
	−0.67±0.08	$n\gamma$	1200±40	300±29	1.858	13500	9.166	3.98	0.0384±0.0029	6.9%	0.256±0.021	0.256±0.021
	−0.86±0.06	$n\gamma$	2146±90	300±38	3.716	7590	9.166	4.24	0.0379±0.0028	7.3%	0.444±0.038	0.441±0.037
	−0.86±0.06	n	673±250	15±4	3.716	400	9.166	4.24	0.297 ±0.014	37.1%	0.383±0.143	
1363	0.80±0.06	$n\gamma$	6115±126	355±19	3.89	9875	13.199	1.21	0.0304±0.0019	5.3%	3.09 ±0.20	3.09 ±0.20
	0.37±0.10	$n\gamma$	3679±116	295±46	1.945	16620	9.166	2.24	0.0473±0.0030	6.4%	1.08 ±0.08	1.07 ±0.07
	0.37±0.10	n	550±58	7±3	3.89	200.7	9.166	2.24	0.327 ±0.011	10.9%	1.04 ±0.12	
	0.02±0.10	$n\gamma$	3843±110	220±38	1.945	13710	9.166	2.91	0.117 ±0.0063	5.0%	0.435±0.027	0.435±0.027
	−0.33±0.10	$n\gamma$	730±31	155±21	1.945	7510	9.166	3.49	0.0418±0.0028	6.9%	0.293±0.023	0.279±0.021
	−0.33±0.10	n	421±90	20±5	3.89	500.1	9.166	3.49	0.306 ±0.014	21.5%	0.211±0.046	
	−0.65±0.08	$n\gamma$	1384±98	290±26	1.945	13170	9.166	3.99	0.0740±0.0047	8.8%	0.158±0.015	0.162±0.015
	−0.65±0.08	n	663±183	30±6	3.89	719.6	9.166	3.99	0.303 ±0.016	27.7%	0.204±0.057	
	−0.87±0.06	$n\gamma$	1652±100	380±27	3.89	9120	9.166	4.32	0.0733±0.0042	7.1%	0.124±0.010	0.124±0.010

V. RESULTS

The differential cross section for charge exchange is calculated from the following formula:

$$\frac{d\sigma}{d\tilde{\Omega}_{\mathrm{CEX}}} = \frac{N_{\mathrm{evts}} - N_{\mathrm{REX}}}{\bar{l}\rho\,\pi^*_{\mathrm{in}} d\Omega_n J f^*} .$$

The numerical value of each of the parameters is given in Table II, where

N_{evts} = number of events, in CEX time-of-flight interval, after adjustment for empty target and random events;

N_{REX} = number of $\pi^- p \to n\gamma$ background events;

π^*_{in} = number of incident pions that traversed the hydrogen target (see below);

$d\Omega_n$ = the geometrical solid angle subtended by the neutron counters;

$\bar{l}\rho$ = the number of target protons per cm^2 seen by an incoming pion, averaged over our pion beam distribution;

J = neutron Jacobian = $d\tilde{\Omega}/d\Omega_{\mathrm{lab}}$;

f^* = the product of all factors which affect our detection efficiency.

In detail, we define f^* as follows:

$$f^* = (1-f_{n\,\mathrm{lost}})(1-f_{\gamma\,\mathrm{conv}})(1-f_{\pi^0\,\mathrm{antis}})(1-f_{\mathrm{antied}})(1-\tfrac{1}{32}N_{\mathrm{out}})\eta_\gamma\eta_n(f_{\mathrm{path}})(1-f_{\gamma\pi^0\,\mathrm{anti}})(1-f_{\mathrm{cont}})(1-f_{\pi\,\mathrm{abs}})(f_{\mathrm{vol}})(1-f_{\mathrm{spark}}),$$

where

$f_{n\,\mathrm{lost}}$ = the fraction of neutrons which are undetected due to scattering in the liquid hydrogen or the target walls, or scattering out of the neutron counter array (varies from 2.7% to 25%);

$f_{\gamma\,\mathrm{conv}}$ = the fraction of CEX events which had a photon convert in the target or the anticounters on the way to the spark chamber (about 7.4%);

$f_{\pi^0\,\mathrm{antis}}$ = the fraction of good CEX events which were lost because of accidentals in the π^0 anticounters (varies from 6% to 8%);

f_{antied} = the fraction of good CEX events which were lost because of accidentals in the target anticounters, $\bar{A}_s$ (varies from 1.5% to 3.7%);

N_{out} = the number of inoperative neutron counters (normally zero);

η_n = the measured efficiency for detecting a neutron which traversed a full counter length (52–40%);

f_{path} = the average fraction of a neutron counter length traversed by the neutrons which passed through the front face of a neutron counter (varies from 0.87 to 0.89);

η_γ = the detection efficiency for a photon which goes in the fiducial volume of the spark chamber (it is taken to be 0.98 over the range of γ energies considered here, as justified in Ref. 18);

$f_{\gamma\pi^0\,\mathrm{anti}}$ = the fraction of good CEX events lost because one photon passed through an $\bar{A}_{\pi^0}$ counter (varies from 18% to 45%);

f_{cont} = the fraction of incident particles which were not pions (varies from 6% to 11%);

$f_{\pi\,\mathrm{abs}}$ = the fraction of pions which were absorbed by interactions in the timing counter and the LH target (1.7%);

f_{vol} = the geometrical acceptance for one photon from π^0 as determined by the fiducial volume of our spark chamber (varies from 12% to 38%);

f_{spark} = the fraction of events lost in the analysis due to our minimal spark requirement for an acceptable photon shower (this correction is either zero or 5%).

The numerical value for every correction factor for every energy and angle is available in Ref. 22. The number of REX events, N_{REX}, was determined from our own measured cross sections. The value of the π^*_{in}'s was calculated by subtracting doubles and randoms from the number of incident beam particles and then multiplying the difference by the fraction of events which were analyzable (usually larger than 0.95). The unanalyzed events are normally associated with film-scanning problems. The value of f^* is dominated by the quantity f_{vol} and $f_{\gamma\pi^0\,\mathrm{anti}}$. The last two factors were evaluated with the same Monte Carlo program which generates CEX and REX events for the REX analysis. In addition to geometry, the factor $f_{\gamma\pi^0\,\mathrm{anti}}$ depends on the efficiency of the π^0 anticounters, discussed in Sec. III D.

The important parameters used in our cross section determination are listed in Table II. The errors in the parameters π^*_{in}, $d\Omega_n$, and J are less than 1% and have not been listed. We did not deem it necessary to obtain the cross section for all the 32 counters separately, so the results for the en-

tire neutron array have been lumped together and averaged. This accounts for the sizable interval in $\cos\tilde{\theta}_{\pi^0}$. The results of our measurements of the CEX differential cross sections for both the n-γ coincidence method and the n-only method are listed in the next to last column of Table II. In general, the agreement between the two methods is satisfactory. The measurements based on the n-γ method have a smaller error than those based on n-only. This is due principally to the fact that the number of CEX events is determined with much greater accuracy by the n-γ method (compare Fig. 5 with Fig. 4), offsetting the uncertainty introduced by demanding a photon in the trigger. The total error in our measurements can be divided into a normalization error and a relative error. The normalization error scales all measurements at each center-of-mass energy in the same way. It is due, e.g., to uncertainty in the beam contamination and the loss of good events because of random noise in the anticounters. It amounts to ±4.8% at $\tilde{E}$ = 1245 MeV, ±4.4% at $\tilde{E}$ = 1337 MeV, and ±3.7% at $\tilde{E}$ = 1363 MeV. The relative error varies for different measurements. It is due, e.g., to counting statistics. The relative error is listed in Table II. Our final result in the cases where there are two measurements is the average, weighted according to the square of the relative error. The error quoted for our cross section values is the normalization error and the weighted relative error combined in quadrature. Our final cross sections are plotted in Fig. 6.

VI. DISCUSSION AND CONCLUSIONS

Recent phase-shift predictions[10-11] for charge exchange at our energies have been included in Fig. 6 with our measurements. In general, there is agreement with the gross features. Our measurements are not sufficiently accurate to distinguish clearly between the four different sets of phase shifts available at $\tilde{E}$ = 1362 MeV. We have made a fit of our data to a Legendre-polynomial expansion; in addition to our measured points, we used a dispersion-relation calculation of the 0° cross section.[23] The coefficients from our fit are given in Table III. Also shown in this table are the following: in column 7, the total cross section obtained by integrating the polynomial; in column 8, the total cross section as measured by others[6,7,24]; and in column 9, the total cross section predicted by the CERN and Saclay phase-shift analyses.[10,11] Our calculated total cross sections depend strongly on the 0° differential cross section calculated by Olsson,[23] to which we assigned an error of 15% at $\tilde{E}$ = 1245 MeV, and 5% at $\tilde{E}$ = 1337 and 1363 MeV.

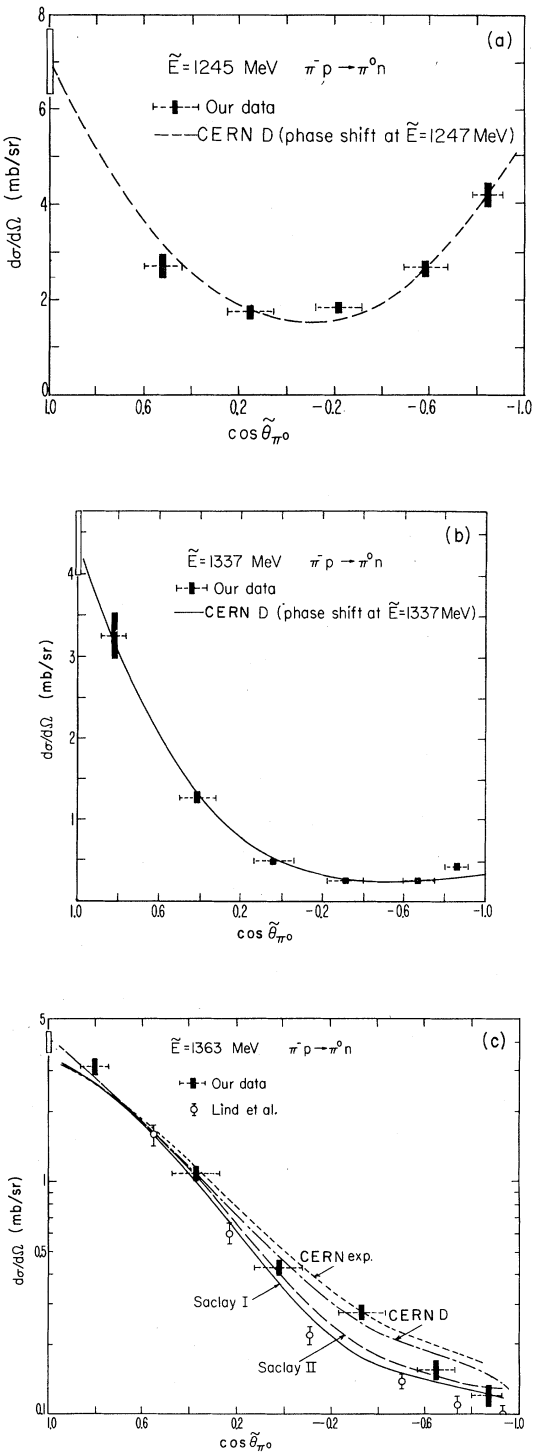

FIG. 6. Differential cross section for $\pi^-p\to\pi^0n$ as a function of $\cos\tilde{\theta}_{\pi^0}$. We have plotted the weighted average of the n-γ coincidence and the n-only measurements. The error plotted includes both the normalization and the relative error. The lines represent the phase-shift predictions, Refs. 10 and 11. Also shown in Fig. 6(c) are the data at $\tilde{E}$ = 1361 MeV of Lind *et al.*, Ref. 7.

The data points indicated by open circles in Fig. 6(c) are the CEX values reported in Ref. 7. They are generally lower than our measurements; the disagreement is largest in the backward direction. We note that the neutron counters used in Ref. 7 were surrounded on four sides by anticounters.

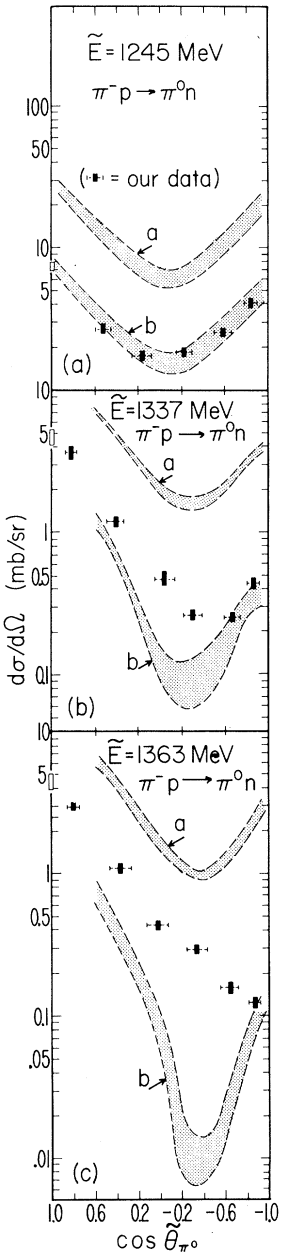

FIG. 7. Our $\pi^- p \to \pi^0 n$ data compared to the bounds of the triangle inequalities $a = \frac{1}{2}(\sqrt{\sigma^+} + \sqrt{\sigma^-})^2$ and $b = \frac{1}{2}(\sqrt{\sigma^+} - \sqrt{\sigma^-})^2$, with $\sigma^\pm = d\sigma/d\Omega(\pi^\pm p \to \pi^\pm p)$. The shaded region at each bound indicates the area of uncertainty due to the uncertainties in the σ^+ and σ^- data, which are taken to be at least 6%.

This has the effect of reducing the cross section because of charged cross scattering, which is particularly important in the backward direction where the neutron energy is the highest.

In Figs. 7(a)–7(c), we have plotted our differential cross sections along with the upper and lower bounds of the CEX cross sections given by the triangle inequalities, Eq. (3). The $\pi^\pm p$ data for the triangle inequalities at $\tilde{E} = 1245$ MeV were obtained by interpolating the CERN phase-shift predictions. At $\tilde{E} = 1337$ MeV we used interpolated values from the data of Rugge and Vik,[25] and at $\tilde{E} = 1363$ MeV we used the data of Ogden *et al.*[26] In calculating the triangle inequalities, we assumed the error in the $\pi^\pm p$ data to be at least 6%, resulting in a region of uncertainty that is given by the shaded area in Fig. 7.

Our data are in agreement with charge independence at all energies and angles, a slight exception being one measurement at $\tilde{E} = 1245$ MeV at $\cos\tilde{\theta}_{\pi^0} = 0.52$. We interpret this mainly as a statistical fluctuation, not unexpected among 27 measurements.

Inspection of Fig. 7 reveals several interesting phenomena. First, the CEX data at $\tilde{E} = 1245$ MeV are consistent with the lower bound of the triangle inequalities over the entire angular region. This is not unexpected, of course, since all phase-shift analyses and theoretical models indicate $A_{3/2} >> A_{1/2}$, due to the dominance of the $\Delta(1236)$ in the region of $\tilde{E} = 1245$ MeV. Second, our measurements at all three energies, when extrapolated to 180°, are consistent with the lower bound of the triangle inequalities. Thus, we fully support the idea of a phase degeneracy at 180° in the π-N system as suggested by Ayed, Bareyre, and Sonderegger. The data at $\tilde{E} = 1363$ MeV are especially interesting in that our CEX data are nowhere near the bounds of the triangle inequalities except in the very backward direction. Thus, the ABS phase degeneracy only holds at 180°, which makes it hard to explain as a dynamical effect due to accidental cancellation of certain amplitudes. Third, it is interesting to note how the CEX data pull away from the lower bound of the triangle inequalities in going from $\tilde{E} = 1245$ to $\tilde{E} = 1363$. This can only be due to the increasing influence of the $A_{1/2}$ amplitude, and, because of the relatively low energy, this is presumably a manifestation of the $P_{11}(1470)$ resonance. The difference between Fig. 7(b) where $\tilde{E} = 1337$ MeV and Fig. 7(c) where $\tilde{E} = 1363$ MeV is particularly striking. Thus, we find it difficult to support the hypothesis of Hauser *et al.*,[27] that the small CEX cross section at 180° in the vicinity of $\tilde{E} = 1400$ MeV is evidence for the P_{11}. We contend that the low backward CEX cross section in the vicinity of $\tilde{E} = 1400$ MeV is a conse-

TABLE III. Legendre coefficients[a] of the least-squares fit to our measurements and the 0° calculation by Olsson.[23] In column 7 is given the total cross section calculated from the Legrendre fit. Column 8 shows total cross-section measurements by others.[6,7,24] Column 9 gives the total cross section calculated from the CERN and Saclay phase-shift analysis.[10,11]

P_π- (MeV/c)	$\tilde{E}$ (MeV)	C_0 (mb/sr)	C_1 (mb/sr)	C_2 (mb/sr)	C_3 (mb/sr)	σ_{tot} (mb) Integrated	σ_{tot} (Other measurements)	σ Phase-shift predictions
317	1245	2.92±0.15	0.09±0.36	2.40±0.36	−0.07±0.29	36.6±2.6	39.5±0.5[b]	40 (CERN)
452	1337	1.07±0.05	1.58±0.12	1.23±0.11	0.25±0.10	13.5±0.8	13.8±0.5[c]	13.8 (CERN)
491	1363	0.99±0.05	1.64±0.11	1.10±0.11	0.41±0.07	12.4±0.8	11.1±0.2[d]	12.4 (CERN-D)
							13.6±0.6[e]	11.1 (Saclay-I)
								11.8 (Saclay-II)

[a] $\frac{d\sigma}{d\Omega} = \sum_{l=0}^{3} C_l P_l(\cos\tilde{\theta}_{\pi^0})$.

[b] Interpolated between $\tilde{E}$=1233 and 1250 MeV (Ref. 24).
[c] Interpolated between $\tilde{E}$=1322 and 1362 MeV (Ref. 7).
[d] $\tilde{E}$=1362 MeV (Ref. 7).
[e] $\tilde{E}$=1363 MeV (Ref. 6).

quence of the ABS phase degeneracy.

ACKNOWLEDGMENTS

The interest and support of Professor K. M. Crowe is gratefully acknowledged, as is the help of Dr. J. A. Helland with the photon spark chamber, and the loan of the vidicon system by Professor V. Perez-Mendez. We appreciate the help of M. Arman, D. Blasberg, J. Comiso, A. Weiss, and R. Belisle during the setup and running of the experiment. We thank J. Vale and the cyclotron crew for the efficient running of the 184-in. synchrocyclotron and dedicated help in various stages of the experiment.

*Work supported in part by the U. S. Atomic Energy Commission.

†Present address: Armed Forces Radiobiology Research Institute, Bethesda, Md. 20014.
‡Present address: Physics Department, Harvard University, Cambridge, Mass. 02138.
§Present address: Physics Department, Yale University, New Haven, Conn. 06520.
‖Present address: Rutherford High Energy Laboratory, Chilton, Berkshire, England.
**Part of this work was done while at the Physics Department, University of California, Los Angeles, Calif. 90024. Present address: Physik-Institut, University of Zurich, Zurich, Switzerland.

[1]P. Berardo, R. Haddock, B. Nefkens, L. Verhey, M. Zeller, A. Parsons, and P. Truoel, Phys. Rev. Letters 24, 419 (1970); 26, 201 (1971).
[2]E. Fermi *et al.*, Phys. Rev. 92, 161 (1953).
[3]M. Glicksman, Phys. Rev. 95, 1045 (1954).
[4]J. Ashkin *et al.*, Phys. Rev. 105, 724 (1957).
[5]V. Zinov *et al.*, Zh. Eksp. Teor. Fiz. 33, 1308 (1957) [Sov. Phys. JETP 6, 1007 (1958)].
[6]J. C. Caris *et al.*, Phys. Rev. 121, 893 (1961).
[7]D. L. Lind *et al.*, Phys. Rev. 138, B1509 (1965).
[8]K. W. Chen *et al.*, Phys. Letters 35B, 257 (1971).
[9]See, for instance, C. Lovelace, in *Proceedings of the International Conference on Elementary Particles, Heidelberg, Germany, 1967,* edited by H. Filthuth (North-Holland, Amsterdam, 1968).
[10]S. Almehed and C. Lovelace, Nucl. Phys. B40, 157 (1972).
[11]R. Ayed *et al.*, Phys. Letters 31B, 598 (1970).
[12]A. Donnachie *et al.*, Phys. Letters 26B, 161 (1968).
[13]D. Feldman, Phys. Rev. 89, 1159 (1953).
[14]A. S. L. Parsons *et al.*, Nucl. Instr. Methods 79, 43 (1970).
[15]N. A. Törnqvist, Nucl. Phys. B6, 187 (1968).
[16]R. Ayed, P. Bareyre, and P. Sonderegger, in Proceedings of the Amsterdam International Conference on Elementary Particles, 1971 (unpublished).
[17]G. C. Oades, in *Springer Tracts in Modern Physics,* edited by G. Höhler (Springer, Berlin, 1970), Vol. 55, and private communication.
[18]P. A. Berardo *et al.* (unpublished); also P. A. Berardo, UCLA Ph. D. thesis, 1970 (unpublished).
[19]S. Andrae, F. Kirsten, T. Nunemaker, and V. Perez-Mendez, LRL Report No. UCRL-11209 (revised), 1964 (unpublished).
[20]A. J. Weiss, B. M. K. Nefkens, and L. J. Verhey, UCLA Internal Report No. 34-P106-33, 1969 (unpublished).
[21]More spectra are given in Ref. 22.
[22]P. A. Berardo *et al.*, UCLA Internal Report No. GN 72-1, 1972 (unpublished).
[23]M. G. Olsson, Phys. Rev. 171, 1681 (1968).
[24]D. V. Bugg *et al.*, Nucl. Phys. B26, 588 (1971).
[25]H. R. Rugge and O. T. Vik, Phys. Rev. 129, 2300 (1963).
[26]P. M. Ogden *et al.*, Phys. Rev. 137, B1115 (1965).
[27]M. G. Hauser *et al.*, Phys. Letters 35B, 252 (1971).